energies

MDPI

Article

Accessible Battery Model with Aging Dependency

Christophe Savard [1], Emiliia Iakovleva [2,*], Daniil Ivanchenko [2] and Anton Rassõlkin [3]

[1] Mainate Labs, rue Notre Dame de l'Oratoire, 43270 Allègre, France; cjs@mainate.com
[2] General Electrical Engineering Department Saint Petersburg Mining University, 2, 21st Line, 199106 St Petersburg, Russia; Ivanchenko_DI@pers.spmi.ru
[3] Department of Electrical Power Engineering and Mechatronics, Tallinn University of Technology, 19086 Tallinn, Estonia; anton.rassolkin@taltech.ee
* Correspondence: yakovleva_ev@pers.spmi.ru; Tel.: +7-921-375-4619

Abstract: Designed to store and discharge electrical energy, rechargeable batteries consist of elementary storage cell assemblies. Aging is affected by various aggravating factors, mainly temperature. There are many electric or electrochemical models which describe their operation. Most standard models do not consider the aging phenomena of batteries and their consequences, while batteries deteriorate when used or stored. Precisely, most battery models do not simulate the influence of cell aging on other cells. The model presented in this paper incorporates aging and the effects of mutual interactions between cells. The model can be established based on four measurement points on the cell characteristic curve and allows the simulation of a single cell's or multiple coupled cells' behavior. The model can then be easily implemented in simulation software like Matlab.

Keywords: battery; electric power storage system; simulation; aging parameters; temperature

check for updates

Citation: Savard, C.; Iakovleva, E.; Ivanchenko, D.; Rassõlkin, A. Accessible Battery Model with Aging Dependency. *Energies* **2021**, *14*, 3493. https://doi.org/10.3390/en14123493

Academic Editors: Carlos Miguel Costa and Teuvo Suntio

Received: 24 April 2021
Accepted: 10 June 2021
Published: 12 June 2021

Publisher's Note: MDPI stays neutral with regard to jurisdictional claims in published maps and institutional affiliations.

Copyright: © 2021 by the authors. Licensee MDPI, Basel, Switzerland. This article is an open access article distributed under the terms and conditions of the Creative Commons Attribution (CC BY) license (https://creativecommons.org/licenses/by/4.0/).

1. Introduction

By nature, electrical energy is not easy to store and nowadays there are several approaches to resolving this problem. Electrical energy can either be stored temporarily in an electrostatic form using supercapacitors [1–3], or be transformed into other types of energy, into mechanical form, with kinetic energy in the flywheels [4], or potential energy in water storages [5] or compressed air [6]. Sometimes, energy is naturally stored in the form of radiant energy in matter. Significant amounts of energy can be stored in thermal form using various methods to keep it in sensible heat, latent heat, or sorption [7–9]. However, electric energy is mainly stored in chemical and electrochemical forms. The main focus of electric energy storage research works is directed towards materials or structures to gain the best storage per mass capacity to condense the most energy in a cell as small and light as possible.

Storage of energy in electrochemical form is achieved by electrochemical cells in the form of primary and secondary (rechargeable) batteries. A primary cell is a battery made to be used once, discarded, and not recharged. Once their energy is depleted, the primary cell must be physically recycled. The rechargeable cell can be charged and discharged several times. The period of charging and subsequent discharging is called a cycle. In both primary and secondary cells, a redox reaction occurs between two electrodes immersed in an electrolyte. A certain amount of electrical energy is accumulated by the cell and is released when an electrically conductive external circuit is connected to its terminals. Generated voltage depends on the electrode's nature. In comparison to primary cells, in rechargeable cells, the chemical reaction is reversed if the cell's current changes direction.

The problem hindering electric energy development as the primary energy source lies in the low amount of power stored in a single cell [10]. Typically, electrochemical rechargeable cells can deliver a maximum current of several amperes under a voltage of one to a few volts. Therefore, electrochemical cells are connected within the batteries in

different ways to meet the user's requirements [11,12]. The separate research branches are focused on the arrangement and control of storage batteries.

Limited energy density is one of the main problems of today's rechargeable batteries. Currently, the best lithium rechargeable batteries reach the energy density of about 240 Wh/kg [13], while gasoline reaches 13.200 Wh/kg. Moreover, gasoline can deliver energy only once, so table wedge calculation indicates that a lithium battery is ecologically more cost-effective than gasoline when it has been cycled more than 55 times. Other technical solutions used in the rechargeable cell are lead-acid and alkaline (NiCd and NiMH) with an energy density of 35 Wh/kg, 100 Wh/kg, and 150 Wh/kg, respectively [14]. There is ongoing research on different ways to improve batteries' performance in terms of power and energy storage density. New technologies aimed at improving materials' energy density by increasing their electrochemical characteristics are being developed by many research groups [15,16]. In research work by Hussain et al. [17], a method for creating high-capacity electrodes using inexpensive means of cation substitution is described. Results obtained in the research are effectively applied in micro digital devices.

To assess the batteries' performance in terms of reliability, energy return, and lifespan, it is essential to have an electrical model simulating cells. The batteries should be modeled with their structure and architecture, considering coupling between cells and the cells' number and arrangement. Since each cell has an individual electrical characteristic, a combination of the cells in a battery may result in an unexpected performance [18]. Different cells in a battery arrangement suffer different stresses and therefore age differently. How et al. in [19] describes the newest state of charge (SoC) estimation for Li-Ion batteries, which is required to increase the service life of batteries and prevent emergencies caused by battery failures. Studies of Lavety and Zhou [20,21] are dedicated to modern problems of rechargeable batteries simulation and estimation of batteries capacity.

It can be seen from literature analysis that, nowadays, the main trends in battery development are increasing life cycle efficiency and reducing mass and dimensions. Such characteristics are also important from the application point of view, such as electric vehicle development [22–24]. The described developments show the study's importance to rechargeable batteries and their optimization based on the simulation of these processes. To simulate the electrical behavior, it is necessary to use a proper equivalent electric model of the battery. Therefore, this paper describes available models of rechargeable batteries.

2. Materials and Methods

2.1. Classical Models of Rechargeable Cells

The open-circuit voltage (OCV) characteristic curve based on battery's SoC is commonly used to describe its characteristics, regardless of cell technology [25]. In a characteristic of $LiFePO_4$ cell shown in Figure 1, the upper flat portion, where the cell's OCV is almost constant (regardless of its charge level), presents the area where the cell should be used. The OCV average value on the upper flat portion depends on the cell technology. For a $LiFePO_4$ cell, the operational voltage is close to 3.3 V, for a lithium-ion cell with electrode this is in the range from 3.3 V to 3.8 V, and for lead-acid it is 2.1 V.

This curve's precise shape depends on individual electrode properties [26] and is usually measured in test conditions starting from a fully charged cell while discharging a part of the stored energy in successive steps. After a sufficient relaxation period [27], generally a few minutes, the cell terminal voltage is measured. Several models accurately describe the electrochemical cell behavior [28]. However, these models are usually accurate for a single cell but do not represent the dynamic battery aging process.

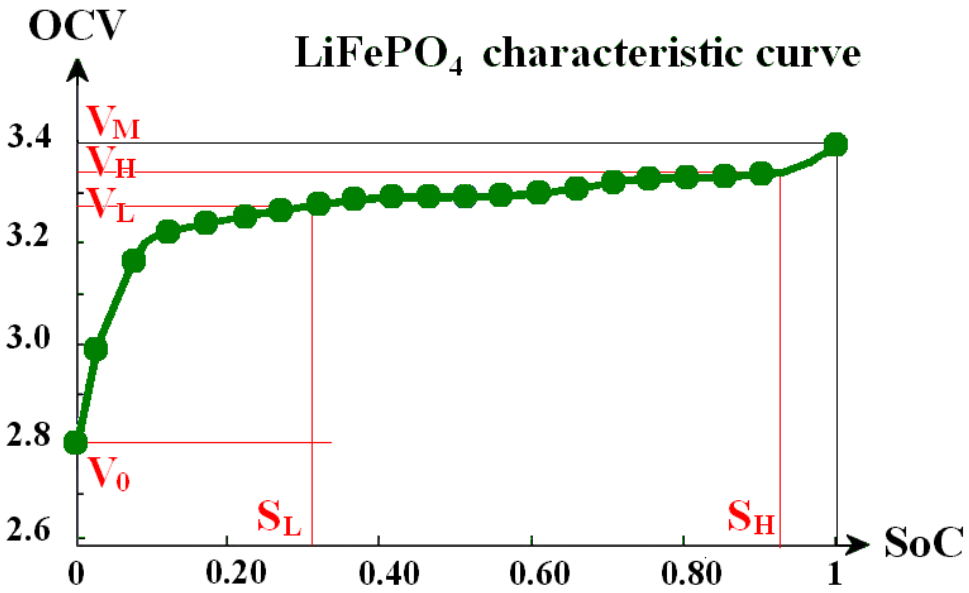

Figure 1. $LiFePO_4$ cell characteristic curve OCV (SoC): V_0—OCV at zero SoC; V_L_OCV at the beginning of linear part; V_H—OCV at the end of linear part; V_M—OCV at full SoC.

Some cell models based on the Thevenin first-order electrical equivalent model, shown in Figure 2, have various improvements. Typically, such models are complete and precise enough to represent the cell behavior and are used in battery management systems (BMSs) for managing the control algorithms of the batteries; moreover, they are used in most simulation software [29]. Electrical series resistance (ESR) incorporates internal voltage drop in current and is specified by electrodes, electrolyte, and fluid resistances related to the terminal nature.

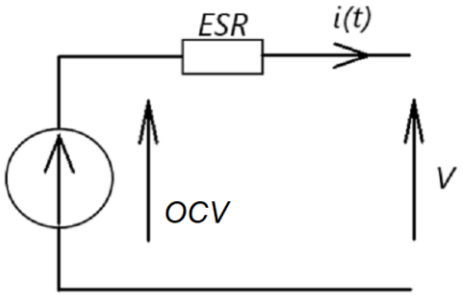

Figure 2. Thevenin's first-order cell electrical equivalent model.

The simplicity of Thevenin's first-order model does not allow to describe all the cell's physical and chemical phenomena. Therefore, the most used model for describing OCV depending on SoC [30] is the Nernst model, represented by Equation (1):

$$V = K_0 + K_1 \ln(\text{SoC}) + K_2 \ln(1 - \text{SoC}) \quad (1)$$

The parameters K_0, K_1, and K_2 are experimentally determined by matching the mathematical model with the actual measured curve. The open-circuit voltage is then an increasing function of SoC.

Other electric models are based on experimental impedance spectroscopy (EIS) techniques [31,32]. The methods are based on adding a low-frequency component to the cell's current and measuring the resulting output voltage. Hence, complex impedance describing the cell is calculated. From this impedance, it is possible to determine the SoC and SoH (state-of-health) of the cell by calculation using Kalman filters [33,34].

To improve any cell model, the implementation of the relaxation phenomenon can be considered [26]. The relaxation phenomenon is the rearrangement of internal chemical reactions after a charge or a discharge, and it is proportional to the capacitance between the two electrodes. Specifically, after a charge, the cell voltage will gradually decrease by a few percent and stabilize at an actual charging OCV. The same phenomenon occurs in discharging phase, where the OCV rises slightly after relaxation for a few minutes. In an electrical equivalent scheme, it can be represented as an additional parallel RC (resistor and capacitor) circuit, in series with the classical model [35]. There also are other types of battery models, such as physics-based models, which can describe the degradation behavior of a battery, which is related to aging [36–39].

The drawback of all mentioned models is their inability to represent the aging phenomena. In all cases, the new model needs to be created after some period of battery usage.

2.2. Aging Process

Rechargeable battery ages in two different manners: calendar and cycle, depending on the battery utilization [40]. This is not the only reason for the battery aging. For example, when gas bubbles are produced in parts of the electrolyte for various reasons [41], the battery will age faster, although to a lesser extent. The calendar aging is secondary to internal phenomena characteristic of the battery after self-discharging [42]. When the cell is not connected to the circuit (stored), the charge will decrease over time. Besides, these phenomena contribute to the gradual reduction of the maximum energy that the cell can store. In this case, the storage temperature is an aggravating factor of aging [43]. The cycle aging reduces the cell performance while a passivation layer is created at the electrode's surface, which may cause internal heating. The cycle aging is temperature dependent [44]; the higher the current flowing through the cell [45], the higher energy is discharged [46]. This aging is reflected by a cell maximum operating charge reduction and ESR increase. After several cycles, the active site number decreases. The metal of the positive electrode wear (loses its porosity), and the resistance between the electrode and the electrolyte increases [47]. Moreover, such factors as overload, deep discharge, and secondary chemical reactions in electrolytes also result in cycle aging [45].

The cell operative charge (also called the capacity of the cell), expressed in ampere-hour (Ah), represents the total energy that a single cell can store. It is noted Q in this paper and is explained by Equation (2). A brand new (just produced) cell has the highest capacity. To determine the capacity, the discharged cell (SoC = 0) is fully charged (SoC = 1) during time $t = t_{max}$. The charge must be carried out until the time t_{max}, when OCV approaches the peak area (V_H on Figure 1), marking an internal thermal runaway.

$$Q = -\int_0^{t_{max}} i(t)dt \tag{2}$$

In this paper, the current that flows out from the cell is considered positive, and the current charging the battery is considered harmful (hence the minus sign in the Equation (2)). SoC of all types of cells expressed in percentage or in per-unit and used to express the cell's remaining charge. The available charge amount in a battery at a time is given by Equation (3), where $Q_0(t)$ is a maximum capacity of the cell and $Q(t)$ is the actual capacity.

$$\mathrm{SoC}(t) = \frac{Q(t)}{Q_0(t)} \tag{3}$$

Since the OCV depends on a SoC, a SoC of 100% corresponds to a maximum voltage (V_M in Figure 1). A SoC of 0% corresponds to the minimum voltage (V_0 in Figure 1); if the OCV drops to that voltage, the cell will suffer irreparable damage. For instance, in lead-acid batteries, when the voltage drops below a minimum value, a non-reversible sulphuration phenomenon occurs. This significantly reduces Q_0. A similar phenomenon

exists in lithium-based cells where a deep discharge can cause damage on the electrodes and can even lead to a polarity reversal.

The SoH defined by Equation (4) reflects the fact that, with age, the cell is no longer able to store as much energy as a new cell.

$$\mathrm{SoH}(t) = \frac{Discharge\ capacity\ (t)}{Discharge\ capacity\ (t=0)} \tag{4}$$

The parameter degradation follows a gradual process, exhibiting no significant regeneration phases. A cell is considered reliable if its SoH is high enough. In practice, this value typically must be higher than 80%. Usually, the maximum storage capacity is the most crucial parameter in energy stored applications, where cells are used. For instance, in the cells used for power supply applications, such as electrical vehicles, the ESR is used for the battery health evaluation [48]. Typically, when ESR is doubled, the cell is considered faulty. That means a SoH of 80% and a doubled ESR corresponds to the cell conventional use limits. Sometimes, in power use cases, the SoH is also defined as the ratio between the ESR at the time concerned and the initial ESR_0 [49]:

$$\mathrm{SoH}(t) = \frac{ESR_0(t)}{ESR} \tag{5}$$

The manufacturers indicate their cells lifespan expressed in cycle number corresponding to the limits. The standard test cycles are carried in laboratory conditions (moderate and constant temperature) and usually do not include deep discharges.

2.3. Modeling a Battery

From the Nernst equation, the simulated curve does not always correspond to the real curve. In the work of Lu et al. [34], an example of a $LiFePO_4$ cell is presented. Several points on the real curve are considered to obtain the model. The accuracy of the model is related to these points. By modeling the OCV curves of this cell, several sets of parameters Ki (for i varying from 0 to 2) can be obtained as a function of the points considered. Table 1 presents two sets of parameters (Case 1 and 2). From the Nernst equation, it can be found that the simulated curve does not always correspond to the actual curve. In this case, Ki parameters represent equilibrium constants of the Nernst equation.

Table 1. k parameter of the Nernst model.

K	K_0	K_1	K_2
Case 1	3.37	0.1	−0.005
Case 2	3.33	0.075	−0.015

In Figure 3, the yellow and red curves (Nernst modeling cases) do not match perfectly with the black curve of actual cell data. However, it is also possible to use a conventional linear regression to fit the curve. Due to the curve inflection point number, a 5th order regression is considered, as shown in Figure 3 by the blue curve, although it does not provide complete matching.

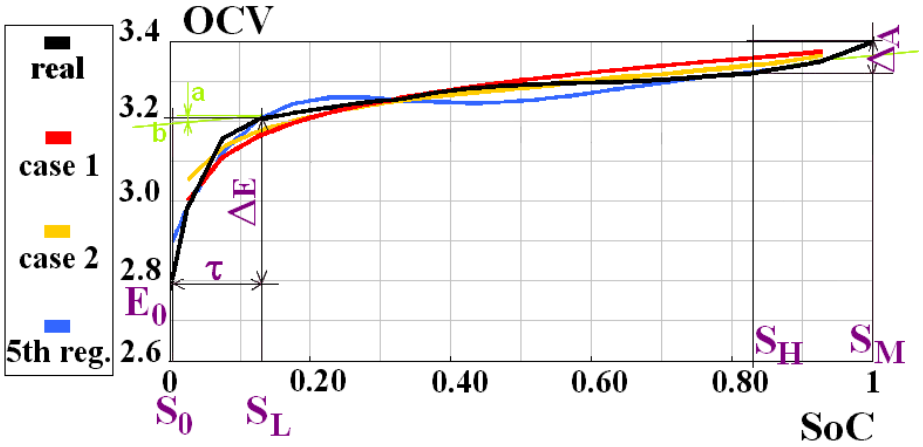

Figure 3. Nernst model applied to a LiFePo4 battery: S_0_empty value of SoC; S_L—minimal value of SoC, for the beginning of linear part of SoC and OCV; τ—low value range of SoC, from S_0 ti S_L; E_0—value of OCV at zero SoC; ΔE—range of OCV for low OCV range; S_H_maximum value of SoC for the linear part; S_M—maximum value of SoC for full charge; ΔA—range of OCV for high OCV range; a, b—parametrs of linear $OCV = aSoC + b$ function.

Since the curve grows continuously, it is possible to divide characteristic into parts with low and high values of SoC, represented by an exponential function (Equations (6) and (7)), and a part with average values of the SoC, represented by a simple linear function (Equation (8)). The resulting equation of $OCV = V^1 + V^2 + V^3$ adds up from three parts V^1, V^2 and V^3, which can be calculated as:

$$V^2 = E_0 + \Delta_0(1 - e^{-\frac{\mathrm{SoC}+S_H}{\tau}}) \quad (6)$$

$$V^3 = \Delta_A \cdot e^{A(\mathrm{SoC}-S_M)} \quad (7)$$

$$V^1 = a\mathrm{SoC} + b \quad (8)$$

For the more precise representation of the model's change zone, the intersections' points should be considered as marked in Figure 4. Due to thermal runaway at high SoCs, resulting in a rise of the curve OCV, obtaining measurements up to the maximum voltage is unlikely. So, four points must be considered on the curve OCV of SoC, which corresponds to the boundaries between the three areas of regular operation and the forbidden zone (for $OCV > V_M$). The names of coordinates are listed in Table 2. The example of setting the remarkable points is represented in Table 3.

Table 2. Definition of the model identification points.

Zones	Deep Discharge	Linear	Runaway	Forbidden
SoC (%)	0	S_L	S_H	100
OCV (V)	V_0	V_L	V_H	V_M

Table 3. Example settings remarkable points.

Zones	Deep Discharge	Linear	Runaway	Forbidden
SoC (%)	0	17.5	77.5	100
OCV (V)	2.600	3.222	3.315	3.400

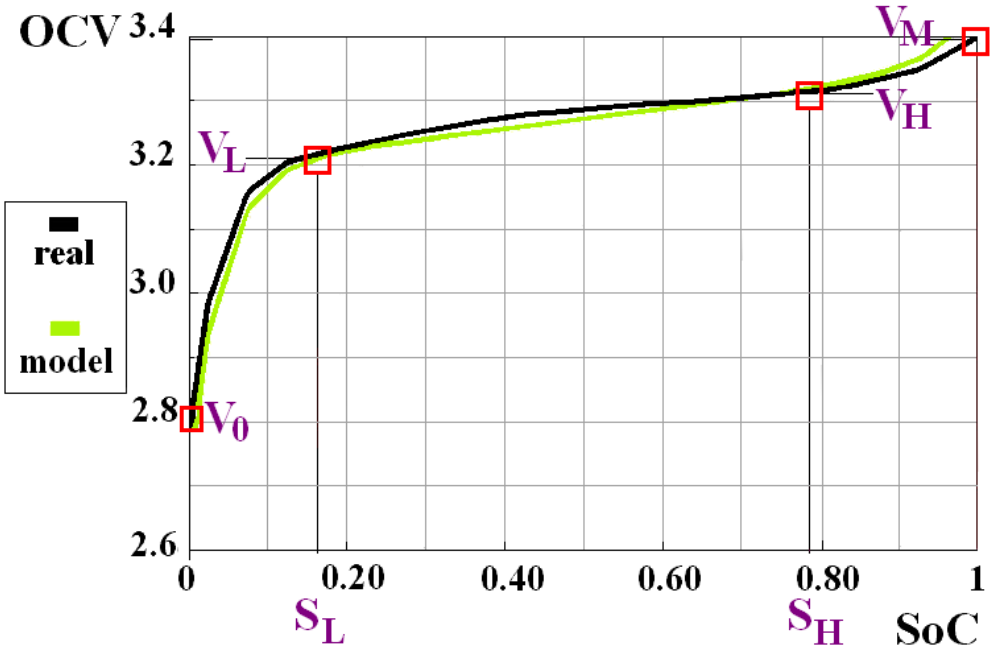

Figure 4. Fitting real curve with the model: V_0—*OCV* at zero SoC; V_L—*OCV* at the beginning of linear part; V_H—*OCV* at the end of linear part; V_M—*OCV* at full SoC.

The resulting model is described by dependence, represented by Equation (9).

$$OCV(\mathrm{SoC}) = \alpha \mathrm{SoC} + \beta + \gamma\left(1 - e^{\frac{-\mathrm{SoC}+S_H}{\zeta}}\right) + \delta e^{\vartheta(\mathrm{SoC}-S_M)} \quad (9)$$

where α, β, γ, and δ are calculated from OCV curve identification points in accordance with Formulas (10)–(13).

$$\alpha = \frac{V_H - V_L}{S_H - S_L} \quad (10)$$

$$\beta = \frac{V_L S_H - V_H S_L}{S_H - S_L} \quad (11)$$

$$\gamma = V_L - V_0 \quad (12)$$

$$\delta = V_M - V_H \quad (13)$$

The parameters ϑ and ζ are empirical and are calculated from available measurements on OCV curve substituted into Equation (5). The estimation of parameter ϑ will be accurate if more measurement points are available for the runaway area (around one to two dozen). Similarly, the better the curve is described, the more precisely ζ parameter, corresponding to an exponential area time constant, will be estimated. The model's application for the data in Table 3 is represented by the Equation (14) and green curve in Figure 4, while the black curve represents actual data.

$$OCV(\mathrm{SoC}) = 2.4729 + 0.155\mathrm{SoC} + 0.6222\left(1 - e^{\frac{-\mathrm{SoC}+0.015}{0.0395}}\right) + 0.08e^{14(\mathrm{SoC}-1)} \quad (14)$$

Instead of the common logarithmic relation between *OCV* and SOC, this model uses an exponential. With available battery lifespan (LS) data from the manufacturer, measured in cycles, corresponding to a minimum-tolerated charging capacity Scrap and considering Scrap is 80% of maximum capacity of the cell Q_0, it is possible to model the decrease of the

maximum capacity Q_0 depending on the number of standard cycles T a cell is subjected to, as represented in Equation (15).

$$Q_0(t) = Q^* \left(1 - Scrap\sqrt{\frac{T}{LS}}\right) \tag{15}$$

In this example, the degradation is assumed to be the square root form according to the principle developed by Lemlich on the remaining time felt [50], which is the case for most physical devices. The square root principle indicates that the more time goes by for an observer, the faster it seems to go for them, and the more the aging phenomenon accelerates. This degradation in the form of a square root of time has already been applied for supercapacitors [51] and batteries [5].

Once the $Q_0(t)$ at each cycle is known, cell electrical parameters can be calculated using Equations (3) for the SoC, (4) for the SoH, and (9) for OCV.

In a simplified way, the electrical series resistance ESR can also be given in proportion to the SoH, considering it doubles from its initial value ESR_0 while SoH passes from 100% to 80%, as represented in Equation (16).

$$ESR(t) = ESR_0 \left(\frac{2 - \mathrm{SoH}(T) - Scrap}{1 - Scrap}\right) \tag{16}$$

This formula allows calculation of discharge depth during the cycle, corresponding to a succession of discharges and charges with possible rest time.

2.4. Simulation of the Aging

The calendar aging process starts when the cell is inactive. Usually, it is characterized by the decrease of a SoH by a few percent [52]. In the developed model, the 5% decrease is considered after 1000 days by default. Table 4 represents the cell self-discharge for various cell technologies. During inactive mode, the cell SoC decreases with time according to the self-discharge value, and this decline can be considered linear.

Table 4. Cell self-discharge as depending on cell technology.

Technology	Lead-Acid	Nickel–Cadmium (*NiCd*)	Nickel Metal Hydride (*NiMH*)	Lithium-Ion	Lithium Iron Phosphate ($LiFePO_4$)
Monthly self-discharge (720 h)	5%	10–20%	15–25%	1–2%	1–3%

SoC evolution depends on the electrical load, and together with relaxation, it forms the open-circuit voltage. The maximum capacity $Q_0(t)$ depends on the SoH, determined by the cell operating conditions. Cycle aging is aggravated by discharge depth in a cycle [46] and the cell temperature [44]. At the same time, calendar aging is aggravated only by the temperature. Therefore, in active mode, the SoH will change from cycle to cycle depending on a battery lifespan LS in accordance with the Equation (17), for each cycle T_i:

$$\mathrm{SoH}(T_i) = \mathrm{SoH}(0) - \sum_{k=1}^{i} \left[\frac{Ad_k At_k \left(T_k^{1/2} - T_{k-1}^{1/2}\right)}{LS^{1/2}}\right] \tag{17}$$

In this formula, worsening parameters Ad and At are related to the depth of discharge and temperature θ and calculated for each cycle k. These parameters can be calculated based on Equations (18) and (19).

$$Ad_k = \left[\frac{\mathrm{SoC}_\mathrm{k}^0 - \mathrm{SoC}_\mathrm{k}^{\min}}{\mathrm{SoC}_\mathrm{k}^0}\right] \tag{18}$$

Here, the $SoC_k{}^0$ is a SoC value at the beginning of the k cycle and the original value before discharge in the k cycle, $SoC_k{}^{min}$ is the minimum value reached by the SoC before recharging, and ρ is the deep of discharge influence parameter, which varies between -1 to 0 depending on how strong the effect of discharge is. The last parameter is empirical and typically has a value -0.25 [53].

$$At_k = e^{\frac{E_a}{K}\left(\frac{1}{273+\theta_{ref}} - \frac{1}{273+\theta_{k-1}}\right)} \tag{19}$$

Here, At parameter follows an Arrhenius law with values for the activation energy E_a range from 0.4 to 1 eV (typically 0.7 eV)/The parameter θ_{ref} in °C is the manufacturer's temperature data given in a reference to *LS*. K is the Boltzmann constant, which is equal to 8617×10^{-5} eV/K.

The relaxation phenomenon can be simulated as a dependence of OCV from SoC in the form of a hysteresis curve [54], as described in detail in [55]. The curves in charging and discharging mode are thus different in its linear portion by a hysteresis voltage, named V$hyst$. For a $LiFePO_4$ cell, hysteresis voltage is about 30 mV [56]. It is also present in Nickel (Ni) cells and has the range of 40–50 mV, but low in the lithium-ion cells [34]. According to research by Thele et al. [54], it is possible to implement voltage hysteresis in a model by adding a term to Equation (9). This term is a positive offset voltage when the battery charges and is harmful if the battery discharges. The model would be improved by considering a non-zero constant time to simulate the current direction's hysteresis fluctuation. The model represented by Equation (9) is simply replaced by the equation (20), where the sign is the function with value 1 if the current *i(t)* is positive and -1 if the current *i(t)* is negative.

$$OCV(\mathrm{SoC}) = \alpha \mathrm{SoC} + \beta + \gamma\left(1 - e^{\frac{-\mathrm{SoC}+S_H}{\varepsilon}}\right) + \delta e^{\vartheta(\mathrm{SoC}-1)} - sgn(i(t))V_{hyst} \tag{20}$$

The cell temperature change must also be considered [57]. Based on research by Damay et al. [58], in a constant current mode, the cell temperature increases almost linearly with time. That is to say, when current returns to zero, the cell temperature turns back to equilibrium, which is an ambient temperature following exponential law. To determine temperature parameters, measurement of the temperature evolution of a cell for different values of the current during charge is required. After the relaxation, the same procedure is taken for the discharge mode. These tests allow for the calculation of entropy-return time constant and proportionality values between temperature and current in charging and discharging modes.

For the first example, the charge constant is 4 °C per hour at nominal current, the discharge constant is 25 °C per hour for nominal current, and the entropy-return time constant is 0.5 h.

3. Results

Using the data presented by Li et al. [34], it is possible to verify the model's operation. Figure 5 shows the evolution of SoC, SoH, open-source voltage, and temperature of the cell, assuming the LS has been deliberately reduced to 100 cycles to see relevant changes in each cycle of the SoC. The cell is cycled as follows: it was discharged to 70% of its capacity under its nominal current, expressed in 1C (1 C-rate current), which takes 2500 s (41 min and 40 s), then recharged during the same period before being placed in relaxation mode. For a simulation of a real operation, cycling charge with 1C is not sufficient to test the battery performance. Nevertheless, to validate the model and check that its behavior is similar to expected, an analysis under this load is sufficient. The ambient temperature θ_a is set at 15 °C. The temperature greatly influences the aging conditions, as recalled in particular in [40]

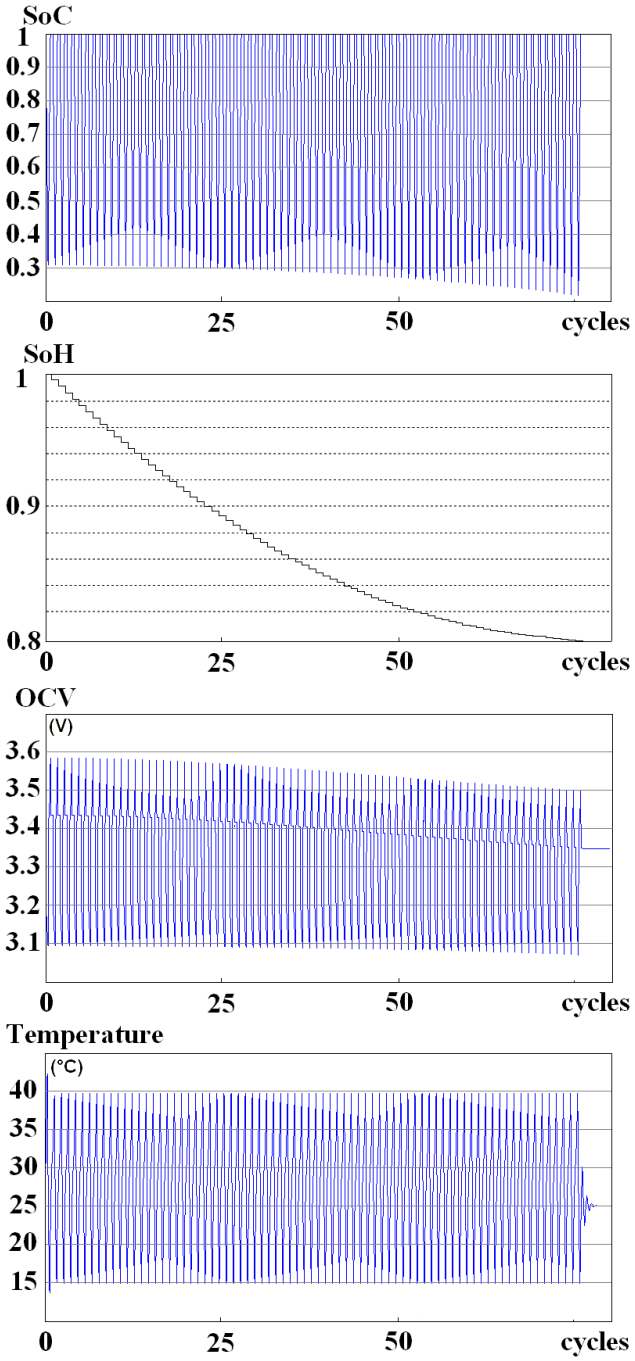

Figure 5. Simulation for the $LiFePO_4$ example, with LS = 100 cycles.

The cell fails after 77 cycles only, essentially because of the temperature. To validate the model, the second example of VL6H lithium cell with experimentally obtained identification points, listed in Table 5, was used.

Table 5. Parameters of a VL6H cell.

Remarkable Points	Deep Discharge	Linear	Runaway	Forbidden
SoC (%)	0	10	86.8	100
OCV (V)	2.925	3.407	3.880	4.010

A comparison of the model (red curve) and measured data (black curve) is represented in Figure 6, where blue curve represents the deep discharge, the yellow curve represents the linear part, and the green curve represents thermal runaway.

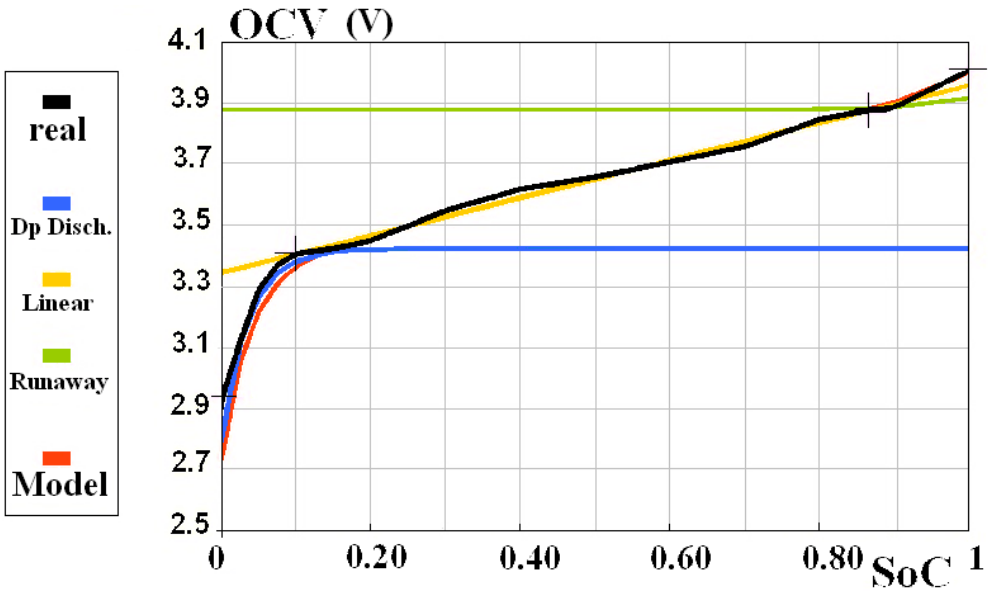

Figure 6. Matching measured and simulated data for the VL6H cell.

Results of the simulation for this single cell with announced L_S of 500 cycles, SoC, SoH, OCV, and temperature curves are presented in Figure 7.

The cell presents a SoH of 80% for 384 cycles only. The premature aging is caused mainly by the depth of discharge (70% initially, almost 80% at its end of life), and the cell temperature reaches a maximum of 42.3 °C.

While the presented model can simulate a cell, it remains to be part of the cell assembly. For this case, the battery can be simulated as four cells connected in parallel. Three of these cells are the basic cells, and the fourth will be a redundant cell. The latter will replace the first cell in case it is no longer able to provide the current. The isolated cell will be the first with its SoC fall to 0, or that the SoH decrease to 0.8. In this case, the cells connected in parallel will self-balance [14]. The simulation stops when a second cell does not fulfill the requirements. To simulate the disparities between cells, the initial conditions differ slightly between each cell: Q *, initial temperature, and ESR_0. For the case of cells from the second example (with L_S = 500), a simulation of SoC, SoH, *OCV*, temperature, *ESR*, and current in each cell is represented in Figure 8. Simulation results for current curves indicate that the redundant cell ensures the balancing of aged cells. The spare cell takes upon the other by providing more current, which speeds up its aging.

Available simulation parameters allow to determine interactions between the cells during the battery life cycle [59,60]. The further development of the model may include the influence of strong currents on aging, similar to Ning et al. in [45], and adjusting the model for energy applications rather than power. Moreover, more detail determining the ESR evolution (or to separate it into two ESR according to the current direction) may be helpful for noticing the positive electrode deterioration kinetic effects, similar to research presented by Bourlot et al. [41].

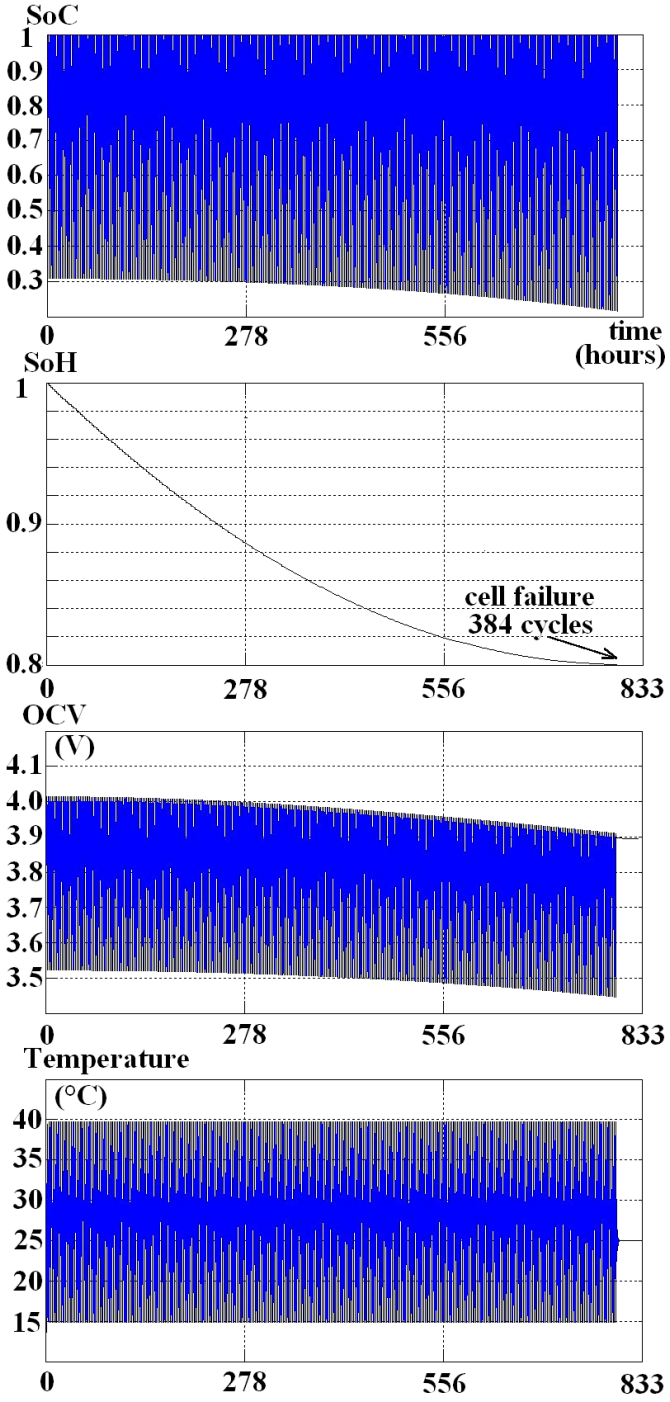

Figure 7. Simulation for a used lithium-ion cell VL6H, with LS = 500 cycles.

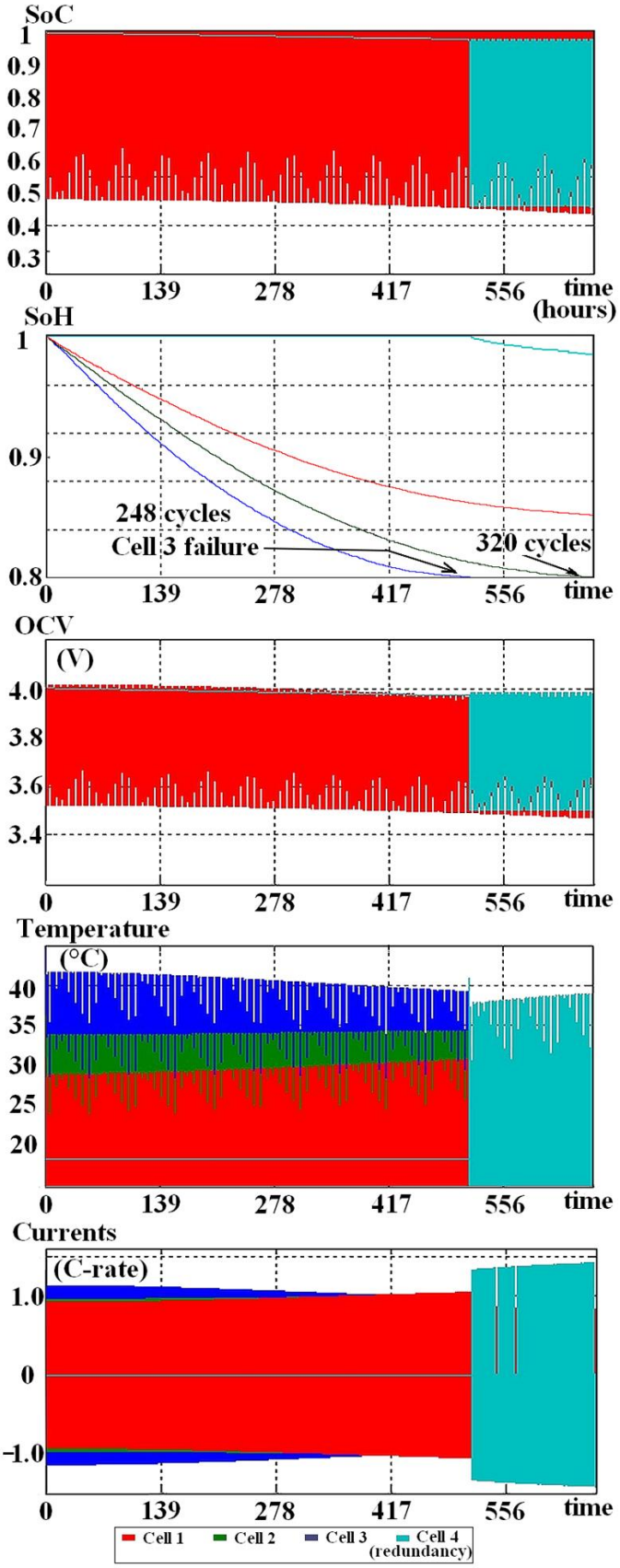

Figure 8. Simulation of a 4-parallel cell mounting.

4. Conclusions

Today, batteries have an important place in the scope of human activities. Uninterruptible power systems, electric vehicles, charging systems, and many other electrical or electromechanical devices are based upon the use of batteries. The increase of energy efficiency, reliability, operational performance, and cost reduction offered by these systems is an extremely important task and the effectiveness of a solution to this problem depends on the simulation accuracy of these systems. Therefore, it is essential to have an ability to select an optimal battery cell structure and to determine cell parameters during the operating life of battery.

To evaluate battery performance, it is important to define the best possible architecture of the cells. For that reason, criteria such as availability, lifespan, or energy efficiency are used. An application of an appropriate mathematical model of the cells with aging parameters integration, as presented in the paper, is an essential tool for development in that field.

The developed simulation model of cells with the implementation of the aging effect, which is described in this study, can be used for the design, calculation, and simulation of battery architecture. The criteria for optimal architecture are the parameters such as accessibility of cells, operating life, and energy efficiency. The advantages of this model are the simplicity of parameter determination as well as applicability for series and parallel connection of different types of cells. The drawback of the model is the difficulty in determining the linear part of the open-circuit voltage curve for some types of cells, but this drawback is common for many similar models.

The simulation result of the developed model is comparable with the more complex Nernst model, which includes the most common values describing the aging of a cell: aging aspect, the influence of temperature, and depth of discharge. These parameters can also be measured and implemented in the model.

Author Contributions: Conceptualization, C.S. and A.R.; methodology, C.S. and E.I.; validation, C.S. and E.I.; formal analysis, D.I.; investigation, C.S. and E.I.; resources, C.S., E.I., A.R., and D.I.; writing—original draft preparation, C.S., D.I., and E.I.; writing—review and editing, A.R. and D.I.; visualization, C.S. and D.I. All authors have read and agreed to the published version of the manuscript.

Funding: The research work by Prof Anton Rassõlkin has been supported by the Estonian Research Council under grant PSG453 "Digital twin for propulsion drive of autonomous electric vehicle".

Acknowledgments: The team of authors acknowledges anonymous reviewers for their feedback, which for sure improved the clarity and quality of this paper.

Conflicts of Interest: The authors declare no conflict of interest.

References

1. Ye, Y.; Cheng, K.W.E. Modeling and Analysis of Series-Parallel Switched-Capacitor Voltage Equalizer for Battery/Supercapacitor Strings. *IEEE J. Emerg. Sel. Top. Power Electron.* **2015**, *3*, 977–983. [CrossRef]
2. Bardanov, A.I.; Vasilkov, O.S.; Pudkova, T.V. Modeling the process of redistributing power consumption using energy storage system with various configurations to align the electrical loads schedule. *J. Phys. Conf. Ser.* **2021**, *1753*, 012013. [CrossRef]
3. Pudkova, T.; Bardanov, A. Principles of electricity metering in networks with non-liner load. *E3S Web Conf.* **2019**, *140*, 07003. [CrossRef]
4. Farhadi, M.; Mohammed, O. Energy Storage Technologies for High-Power Applications. *IEEE Trans. Ind. Appl.* **2016**, *52*, 1953–1961. [CrossRef]
5. Tseng, K.H.; Shum, C.K.; Kim, J.-W.; Wang, X.; Zhu, K.; Cheng, X. Integrating Landsat Imageries and Digital Elevation Models to Infer Water Level Change in Hoover Dam. *IEEE J. Sel. Top. Appl. Earth Obs. Remote Sens.* **2016**, *9*, 1696–1709. [CrossRef]
6. Pickard, W.F. Massive Electricity Storage for a Developed Economy of Ten Billion People. *IEEE Access* **2015**, *3*, 1392–1407. [CrossRef]
7. Jia, Q.S.; Shen, J.X.; Xu, Z.B.; Guan, X.H. Simulation-Based Policy Improvement for Energy Management in Commercial Office Buildings. *IEEE Trans. Smart Grid* **2012**, *3*, 2211–2223. [CrossRef]
8. Bazhin, V.Y.; Kuskov, V.B.; Kuskova, Y.V. Problems of using unclaimed coal and other carbon-containing materials as energy briquettes. *Ugol* **2019**, *4*, 50–54. [CrossRef]

9. Bezyazychnyi, V.F.; Szcerek, M.; Pervov, M.L.; Timofeev, M.V.; Prokofiev, M.A. The Study of the Effect of Temperature on the Ability of Metals to Accumulate Energy during Their Plastic Deformation. *J. Min. Inst.* **2019**, *235*, 55–59. [CrossRef]
10. Belskiy, A.A.; Dobush, V.S.; Haikal, S.F. Operation of a Single-phase Autonomous Inverter as a Part of a Low-power Wind Complex. *J. Min. Inst.* **2019**, *239*, 564–569. [CrossRef]
11. Ci, S.; Lin, N.; Wu, D. Reconfigurable battery techniques and systems: A survey. *IEEE Access* **2016**, *4*, 1175–1189. [CrossRef]
12. Maharjan, L.; Yamagishi, D.; Akagi, H. Active-Power Control of Individual Converter Cells for a Battery Energy Storage System Based on a Multilevel Cascade PWM Converter. *IEEE Trans. Power Electron.* **2012**, *27*, 1099–1107. [CrossRef]
13. Chemali, E.; Preindl, M.; Malysz, P.; Emadi, A. Electrochemical and Electrostatic Energy Storage and Management Systems for Electric Drive Vehicles: State-of-the-Art Review and Future Trends. *IEEE J. Emerg. Sel. Top. Power Electron.* **2016**, *4*, 1117–1134. [CrossRef]
14. Savard, C. *Le Stockage de l'Énergie Électrique*; du Mainate, L.E., Ed.; Universitaires Européennes: Paris, France, 2017.
15. Redozubov, S.S.; Nenasheva, E.A.; Gaidamaka, I.M.; Zaitseva, N.V. Low-Temperature Ceramic Materials Based on Pyrochlore Compounds in the Bi_2O_3–ZnO–Nb_2O_5 System. *Inorg. Mater.* **2020**, *56*, 77–82. [CrossRef]
16. Bazhin, V.Y.; Aleksandrova, T.A.; Kotova, E.L.; Suslov, A.P. A modern View of Anomalies in the Metal Groups of the Periodic System of D.I.Mendeleev. *J. Min. Inst.* **2019**, *239*, 520–527. [CrossRef]
17. Hussain, I.; Hussain, T.; Lamiel, C.; Zhang, K. Turning indium oxide into high-performing electrode materials via cation substitution strategy: Preserving single crystalline cubic structure of 2D nanoflakes towards energy storage devices. *J. Power Sources* **2020**, *480*, 228873. [CrossRef]
18. Jaguemont, J.; Dube, Y.; Bouton, L. Characterization and Modeling of a Hybrid-Electric-Vehicle Lithium-Ion Battery Pack at Low Temperatures. *IEEE Trans. Veh. Technol.* **2016**, *65*, 1–14. [CrossRef]
19. How, D.N.T.; Hannan, M.A.; Hossain Lipu, M.S.; Ker, P.J. State of Charge Estimation for Lithium-Ion Batteries Using Model-Based and Data-Driven Methods: A Review. *IEEE Access* **2019**, *7*, 136116–136136. [CrossRef]
20. Lavety, S.; Keshri, R.; Ghosh, S.; Chaudhari, M.A. Non-Linear Model and Parameter Extraction for Charge/discharge Behavior of Valve Regulated Lead-Acid Battery. *IEEE Trans. Energy Convers.* **2021**. [CrossRef]
21. Zhou, Z.; Cui, Y.; Kong, X.; Li, J.; Zheng, Y. A fast capacity estimation method based on open circuit voltage estimation for LiNixCoyMn1-x-y battery assessing in electric vehicles. *J. Energy Storage* **2020**, *32*, 101830. [CrossRef]
22. Rassõlkin, A.; Sell, R.; Leier, M. Development case study of first Estonian Self-driving car ISEAUTO. *Sci. J. Riga Tech. Univ.-Electr. Control. Commun. Eng.* **2018**, *14*, 81–88. [CrossRef]
23. Shklyarskiy, Y.E.; Lutonin, A.S.; Palyanicin, P.S. PMSM control system with open-end winding and floating bridge capacitor. *IOP Conf. Ser. Mater. Sci. Eng.* **2019**, *643*, 012084. [CrossRef]
24. Zhukovskiy, Y.L.; Suslikov, P.K.; Russkih, N.I.; Korolev, N.A. The use of vehicle-to-grid technology for the integration of electric vehicles in the power system of the city. *J. Phys. Conf. Ser.* **2019**, *1333*, 062032. [CrossRef]
25. Roscher, M.; Sauer, D.U. Dynamic electric behavior and open-circuit-voltage modeling of LiFePO4-based lithium ion secondary batteries. *J. Power Sources* **2011**, *196*, 331–336. [CrossRef]
26. Petzl, M.; Danzer, M.A. Advancements in OCV Measurement and Analysis for Lithium-Ion Batteries. *IEEE Trans. Energy Convers.* **2013**, *28*, 675–681. [CrossRef]
27. Pei, L.; Lu, R.; Zhu, C. Relaxation model of the open-circuit voltage for state-of-charge estimation in lithium-ion batteries. *IET Electr. Syst. Transp.* **2013**, *3*, 112–117. [CrossRef]
28. Zhang, C.; Li, K.; Mcloone, S.; Yang, Z. Battery Modelling Methods for Electric Vehicles—A Review. In Proceedings of the IEEE European Control Conference (ECC), Strasbourg, France, 24–27 June 2014; pp. 2673–2678.
29. Cacciato, M.; Nobile, G.; Scarcella, G.; Scelba, G. Real-Time Model-Based Estimation of SOC and SOH for Energy Storage Systems. *IEEE Trans. Power Electron.* **2017**, *32*, 794–803. [CrossRef]
30. Liu, X.L.; Qin, S.X.; He, Y.; Zheng, X.X.; Cao, C.R. SOC estimation of the lithium-ion battery with the temperature-based Nernst model. In Proceedings of the IEEE 2016 IEEE 8th International Power Electronics and Motion Control Conference (IPEMC-ECCE Asia), Hefei, China, 22–26 May 2016; pp. 1419–1422.
31. Seaman, A.; Dao, T.S.; McPhee, J. A survey of mathematics-based equivalent circuit and electro-chemical battery models for hybrid and electric vehicle simulation. *J. Power Sources* **2014**, *256*, 410–423. [CrossRef]
32. Semenov, K.N.; Letenko, D.G.; Charykov, N.A.; Letenko, D.G.; Nikitin, V.A.; Keskinov, V.A.; Matuzenko, M.Y.; Kopyrin, A.A. Synthesis and identification of fullerenol prepared by the direct oxidation route. *Russ. J. Appl. Chem.* **2010**, *83*, 2076–2080. [CrossRef]
33. Haifeng, D.; Xuezhe, W.; Zechang, S. A new SOH prediction concept for the power lithium-ion battery used on HEVs. In Proceedings of the IEEE 2009 IEEE Vehicle Power and Propulsion Conference, Dearborn, MI, USA, 7–9 September 2009; pp. 1649–1653.
34. Lu, L.; Han, X.; Li, J.; Hua, J.; Ouyang, M. A review on the key issues for lithium-ion battery management in electric vehicles. *J. Power Sources* **2013**, *226*, 272–288. [CrossRef]
35. Xiong, R.; He, H.; Guo, H.; Ding, Y. Modeling for Lithium-Ion Battery used in Electric Vehicles. *Procedia Eng.* **2011**, *15*, 2869–2874. [CrossRef]
36. Paarmann, S.; Cloos, L.; Technau, J.; Wetzel, T. Measurement of the Temperature Influence on the Current Distribution in Lithium-Ion Batteries. *Energy Technol.* **2021**, 2000862. [CrossRef]

37. Li, Y.; Vilathgamuwa, M.; Choi, S.-S.; Farrell, T.W.; Tran, N.-T.; Teague, J. Development of a degradation-conscious physics-based lithium-ion battery model for use in power system planning studies. *Appl. Energy* **2019**, *248*, 512–525. [CrossRef]
38. Unagar, A.; Tian, Y.; Chao, M.A.; Fink, O. Learning to Calibrate Battery Models in Real-Time with Deep Reinforcement Learning. *Energies* **2021**, *14*, 1361. [CrossRef]
39. Cuadras, A.; Miró, P.; Ovejas, V.J.; Estrany, F. Entropy generation model to estimate battery ageing. *J. Energy Storage* **2020**, *32*, 101740. [CrossRef]
40. Broussely, M.; Biensan, P.; Bonhomme, F.; Blanchard, P.; Herreyre, S.; Nechev, K.; Staniewicz, R.J. Main aging mechanisms in Li ion batteries. *J. Power Sources* **2005**, *146*, 90–96. [CrossRef]
41. Bourlot, S.; Blanchard, P.; Robert, S. Investigation of aging mechanisms of high power Li-ion cells used for hybrid electric vehicles. *J. Power Sources* **2011**, *196*, 6841–6846. [CrossRef]
42. Yazami, R.; Reynier, Y.F. Mechanism of self-discharge in graphite-Lithium anode. *Electrochim. Acta* **2002**, *47*, 1217–1223. [CrossRef]
43. Dubarry, M.; Devie, A. *Battery Cycling and Calendar Aging: Year One Testing Result*; University of Central Florida. Electric Vehicle Transportation Center (EVTC): Cocoa, FL, USA, 2016.
44. Bloom, I.; Cole, B.W.; Sohn, J.J.; Jones, S.A.; Polzin, E.G.; Battaglia, V.S.; Henriksen, G.L.; Motloch, C.; Richaardson, R.; Unkelhaeuser, Y.; et al. An Accelerated calendar and cycle life study of Li-ion cells. *J. Power Sources* **2001**, *101*, 238–247. [CrossRef]
45. Ning, G.; Haran, B.; Popov, B.N. Capacity fade study of lithium-ion batteries at high discharge rates. *J. Power Sources* **2003**, *117*, 160–169. [CrossRef]
46. Sauer, D.U.; Wenzl, H. Comparison of different approaches for lifetime prediction of electro-chemical systems—Using lead-acid batteries as example. *J. Power Sources* **2008**, *176*, 534–546. [CrossRef]
47. Hausmann, A.; Depcik, C. Expanding the Peukert equation for battery capacity modeling through inclusion of a temperature dependency. *J. Power Sources* **2013**, *235*, 148–158. [CrossRef]
48. Lievre, A.; Sari, A.; Venet, P.; Hijazi, A.; Ouattara-Brigaudet, M.; Pelissier, S. Practical Online Estimation of Lithium-Ion Battery Apparent Series Resistance for Mild Hybrid Vehicles. *IEEE Trans. Veh. Technol.* **2016**, *65*, 4505–4511. [CrossRef]
49. Le, D.; Tang, X. Lithium-ion Battery State of Health Estimation Using Ah-V Characterization. In Proceedings of the Annual Conference of the Prognostics and Health Management Society, Montreal, QC, Canada, 25–29 September 2011; pp. 1–7.
50. Lemlich, R. Subjective acceleration of time with aging. *Percept. Mot. Ski.* **1975**, *41*, 235–238. [CrossRef] [PubMed]
51. Shili, S.; Hijazi, A.; Sari, A.; Lin-Shi, X.; Venet, P. Balancing circuit new control for supercapacitor storage system lifetime maximization. *IEEE Trans. Power Electron.* **2017**, *32*, 4939–4948. [CrossRef]
52. Eddahech, A. Modélisation du vieillissement et détermination de l'état de santé de batteries lithium-ion pour application véhicule électrique et hybride. Doctoral Dissertation, Université Sciences et Technologies-Bordeaux I, Talence, France, 2013. (In French)
53. Soussens, M.; Laulheret, R.; Cabardaye, A. Modeles de degradation des batteries d'accumulateurs. In Proceedings of the 19th Congres de Maitrise des Risque et Surete de fonctionnement, Dijon, France, 21–23 October 2014; CNES: Paris, France, 2014. (In French)
54. Thele, M.; Bohlen, O.; Sauer, D.U.; Karden, E. Development of a voltage-behavior model for NiMH batteries using an impedance-based modeling concept. *J. Power Sources* **2008**, *175*, 635–643. [CrossRef]
55. Gerschler, J.B.; Sauer, D.U. Investigation of Open-Circuit-Voltage Behaviour of Lithium-Ion Batteries with Various Cathode Materials under Special Consideration of Voltage Equalisation Phenomena. In Proceedings of the International Battery, Hybrid and Fuel Cell Electric Vehicle Symposium EVS24, Stavanger, Norway, 13–16 May 2009.
56. Malik, R.; Abdellahi, A.; Ceder, G. A Critical Review of the Li Insertion Mechanisms in LiFePO4 Electrodes. *J. Electrochem. Soc.* **2013**, *160*, A3179–A3197. [CrossRef]
57. Khan, S.; Shahzad, M.; Habib, U.; Gawlik, W.; Palensky, P. Stochastic battery model for aggregation of thermostatically controlled loads. In Proceedings of the 2016 IEEE International Conference on Industrial Technology (ICIT), Taipei, Taiwan, 14–17 March 2016; pp. 570–575.
58. Damay, N.; Friedrich, G.; Forgez, C. Modélisation thermique en vue du dimensionnement d'un pack batterie, avec prise en compte du couplage électro-thermique pour la caractérisation des pertes éelectriques. In Proceedings of the Symposium de Genie Electrique, Grenoble, France, 7–9 June 2016. (In French)
59. Abramovich, B.N.; Ustinov, D.A.; Abdallah, W.J. Development and design of a mobile power plant in the form of a standalone power supply. *J. Phys. Conf. Ser.* **2021**, *1753*, 012006. [CrossRef]
60. Korolev, N.; Solovev, S. Monitoring the technical condition of autonomous electrical systems with electric drive. *E3S Web Conf.* **2019**, *140*, 04015. [CrossRef]